

# Infrared Signature of Structural Isomers of Gas– Phase $M^+(N_2O)_n$ ( $M = Cu, Ag, Au$ ) Ion–Molecule Complexes

*Ethan M. Cunningham, Alexander S. Gentleman, Peter M. Beardsmore, Andreas Iskra, and  
Stuart R. Mackenzie\**

Department of Chemistry, University of Oxford, Physical and Theoretical Chemistry  
Laboratory, South Parks Road, Oxford, OX1 3QZ, United Kingdom

\*Corresponding Author:      [stuart.mackenzie@chem.ox.ac.uk](mailto:stuart.mackenzie@chem.ox.ac.uk)

## Abstract

Gas-phase metal ion–ligand complexes offer model environments to study molecular interactions which are key to many catalytic processes. Here, we present a combined experimental and computational study of  $M^+(N_2O)_n$  [ $M = Cu, Ag, Au$ ;  $n = 2-7$ ] complexes. The spectra provide clear evidence for both nitrogen– and oxygen– bound ligands giving rise to a wide range of structural isomers for each complex studied. The evolution of the complex structures observed as well as spectral trends for each metal center are interpreted in terms of a molecular orbital binding picture and resulting calculated ligand binding energies. Given the environmental importance of nitrogen oxides, these results have implications for metal–catalysed removal of nitrous oxide and, particularly, the prospect of initiating infrared–driven isomer–selective chemistry in size–selected complexes.

## Introduction

The use of metal–ligand complexes is widespread in chemistry, both as prototypes for bonding in inorganic and organometallic chemistry, and as pivotal species in a wide variety of catalytic processes. The investigation of gas–phase metal ion complexes offers the prospect of gaining a deeper understanding of key metal–ligand interactions, ligand activation and metal ion solvation, all fundamental processes in chemistry, biology, geochemistry and astrophysics.<sup>1-2</sup> Of particular note, the role of gas–phase metal–ligand complexes as models of reaction intermediates has been studied extensively both experimentally and theoretically.<sup>3-5</sup>

The ligand of interest in this work, nitrous oxide, is a potent greenhouse gas,<sup>6</sup> accounting for 5 % of anthropogenic greenhouse emissions, and is a major factor in the depletion of stratospheric ozone.<sup>7-8</sup> Accordingly, there is considerable interest in reducing N<sub>2</sub>O levels using metal–catalyzed N<sub>2</sub>O decomposition / reduction for which M<sup>+0/-</sup>(N<sub>2</sub>O)<sub>n</sub> complexes represent model entrance-channel species.<sup>9</sup> To this end, extensive studies of N<sub>2</sub>O reactions with atomic metal cations have been performed and reviewed by Lavrov *et al.*,<sup>10</sup> and by Böhme and Schwarz.<sup>5</sup> It is clear that N<sub>2</sub>O can act as both an O and N source for atomic cations, leading to oxide and nitride formation.<sup>10</sup> Theoretical studies of N<sub>2</sub>O interactions with neutral atomic metal centers support O–coordination of N<sub>2</sub>O,<sup>11-13</sup> but matrix isolation infrared studies report N–coordination to metal centers such as Ni, Pd, Pt and MCl (M = Cu, Ag).<sup>14-15</sup> The gas–phase reactivity of nitrous oxide with metal ions and clusters has been studied by several groups,<sup>16-24</sup> but relevant gas–phase infrared spectroscopy of N<sub>2</sub>O complexes is limited to pure (N<sub>2</sub>O)<sub>n</sub><sup>+/-</sup> complexes;<sup>25,26</sup> free electron laser studies of N<sub>2</sub>O on Rh<sub>n</sub><sup>+</sup> clusters;<sup>27-29</sup> and blackbody infrared radiative dissociation.<sup>30</sup> The studies of N<sub>2</sub>O on metal clusters demonstrated the ability to drive decomposition of the nitrous oxide on size–selected clusters (with resulting N<sub>2</sub> loss) using resonant infrared excitation. In this sense the decorated cluster

represents an entrance–channel complex on the reactive potential energy surface. The ability to tune reactivity from such pre–reactive states to produce non–statistical reaction dynamics represents a long–standing goal in cluster science.<sup>31</sup>

There remains a relative lack of information on gas-phase  $M^{+/0-}N_2O$  complexes from which trends in binding energies / motifs might be extrapolated. Such studies offer the promise of detailed insight into the intricacies of O– and N–binding of  $N_2O$  to metal centers. One such experimental technique that has been readily used to probe isolated gas-phase metal–ligand complexes is infrared resonance–enhanced photodissociation (IR–REPD) spectroscopy. Adopted early for the study of metal–ligand complexes by Lisy and co-workers (for studies of  $M^+H_2O$ <sup>32-33</sup> and  $M^+CH_4$ <sup>34</sup> complexes), IR–REPD has been employed by several groups worldwide and often provides exquisite insight into the structures of gas–phase metal–ligand complexes.<sup>1</sup> Here, we present the results of a detailed IR–REPD investigation of gas-phase  $M^+(N_2O)_n$  complexes ( $M = Cu, Ag, Au$ ) supported by quantum chemical calculations of energetically low–lying structures and spectral simulations.

## Experimental

The instrument and technique employed in these studies have been described in detail recently<sup>35</sup> and only brief details are given here. Gas-phase  $M^+(N_2O)_n$  ( $M = Cu, Ag, Au$ ) complexes and their argon-tagged analogues are formed by 532 nm pulsed laser ablation of a rotating metal disc in the presence of Ar carrier gas seeded with 0.6 – 1.5 %  $N_2O$ . The resulting molecular / cluster beam is skimmed and charged species are detected by linear time-of-flight mass spectrometry. Tuneable pulsed infrared radiation in the region 2200-2400  $cm^{-1}$  – covering the asymmetric (or N=N) stretch in  $N_2O$  – is provided by an optical parametric oscillator/amplifier system (LaserVision). The infrared beam counter-propagates with the molecular beam and spectra are collected using the ‘inert messenger’ technique,<sup>36-37</sup> in which the loss of a weakly-bound Ar atom from  $M^+(N_2O)_n$ -Ar complexes provides the signature of IR-photon absorption as a function of wavenumber.

To aid in the assignment and interpretation of the experimental data, the structures and infrared spectra of energetically low-lying isomers have been calculated using density functional theory (DFT) employing the B3P86 hybrid density functional<sup>38</sup> coupled with the Def2TZVP basis set.<sup>39-40</sup> All calculations were performed using the Gaussian09 suite of programs.<sup>41</sup> Further details, including structures and coordinates for the putative global minima structures of all complexes, together with composite simulated spectra, potential energy surfaces for the  $n = 1$  complexes and molecular orbital diagrams can be found in the supporting information associated with this article.

## Results and Discussion

### Overview

Figure 1 shows a typical time-of-flight mass spectrum illustrating the production of  $\text{Au}^+(\text{N}_2\text{O})_n$  complexes following ablation of a gold target in the presence of an argon carrier gas seeded with 0.6%  $\text{N}_2\text{O}$ .  $\text{Au}^+(\text{N}_2\text{O})_n$  complexes and their Ar-tagged counterparts are clearly identifiable. The range of complexes generated can be controlled to some degree *via* the partial pressure of  $\text{N}_2\text{O}$  and the backing pressure behind the pulsed valve. Additional peaks in the mass spectrum (indicated with asterisks in Figure 1) are assigned to mixed  $\text{M}^+(\text{N}_2\text{O})_m(\text{H}_2\text{O})_{1,2}$  complexes arising from contaminant background  $\text{H}_2\text{O}$  which are beyond focus of the present study.

The infrared spectra of the Ar-tagged  $\text{M}^+(\text{N}_2\text{O})_{n=2-7}$  ( $\text{M}=\text{Cu}, \text{Ag}, \text{Au}$ ) complexes are shown in Figure 2, recorded by monitoring the Ar atom loss from the parent ion as a function of IR wavenumber. In each case, two distinct bands are observed: one close to the N=N stretching frequency (or  $\text{N}_2\text{O}$  asymmetric stretch) of free  $\text{N}_2\text{O}$  at  $2223.5\text{ cm}^{-1}$ ,<sup>42</sup> and the other significantly blue-shifted by between  $50$  and  $140\text{ cm}^{-1}$ . The former shows comparatively weak dependence on the number of ligands attached, except for a narrowing of the band and a small shift (*ca.*  $20\text{ cm}^{-1}$ ) towards the free  $\text{N}_2\text{O}$  stretch as  $n$  increases. The variation of this band with  $n$  is essentially identical for the three metals studied here.

By contrast, the more blue-shifted band exhibits a more pronounced size-dependence which differs for the three metal ions studied. For the  $\text{Cu}^+(\text{N}_2\text{O})_n\text{-Ar}$  and  $\text{Ag}^+(\text{N}_2\text{O})_n\text{-Ar}$  series, a 40% reduction in the blue-shift from the free  $\text{N}_2\text{O}$  is observed between  $n = 2$  and  $n = 4$  (from  $110\text{ cm}^{-1}$  to  $67\text{ cm}^{-1}$ , and  $80$  to  $47\text{ cm}^{-1}$ , respectively). In the case of  $\text{Au}^+(\text{N}_2\text{O})_n\text{-Ar}$ , however, the blue-shift is larger (at  $140\text{ cm}^{-1}$ ) and the band shifts minimally (by *ca.*  $15\text{ cm}^{-1}$ ) as  $n$  increases.

## $M^+(N_2O)$ and $M^+(N_2O)_2$

The first understanding of the observed spectra is provided by the  $M^+-N_2O$  potential energy surfaces. Figure 3a) shows the calculated potential energy surface (PES) for the  $Au^+N_2O$  complex illustrating a linear  $Au^+NNO$  (*i.e.*, N-bound) putative global minimum structure with a pronounced secondary minimum corresponding to the bent O-bound isomer. The angular plot, Figure 3 b), shows the two minima separated by a barrier to internal rotation of almost 1 eV. During the clustering process within the molecular beam expansion, it is highly likely that excited isomeric forms will be trapped behind such barriers leading to the presence of isomers with both N-bound and O-bound ligands. It is equally clear, that within each of these minima, ligands are free to undergo wide-amplitude motion. In what follows, the numbers of N- and O-bound ligands in a particular  $M^+(N_2O)_n$  complex are represented using the notation  $N^xO^y$ , where  $x$  and  $y$  represent integer values and  $x + y = n$  such that  $N^1O^2$  is an isomer of  $M^+(N_2O)_3$  with one N-bound and two O-bound ligands.

The interpretation of multiple isomers is supported by DFT spectral simulations of the infrared spectra recorded. Figure 4 shows a comparison of the experimental IR spectra of  $M^+(N_2O)_2-Ar$  complexes with spectral simulations of energetically low-lying structural isomers of the singlet electronic ground state. In each case, the doubly N-bound  $N^2$  isomer (structures IA, IB, IC) represents the putative global minimum structure with the  $N^1O^1$  (IIA, IIB, IIC) and  $O^2$  (IIIA, IIIB, IIIC) isomers representing higher-lying local minima (see Supporting Information for more details). It is clear that the  $N^2$  global minimum structure cannot account for the two spectral bands observed and that O-bound ligands must be present.

The origin of the two bands in the observed spectra is clear: The band around  $2240\text{ cm}^{-1}$  in each complex arises from isomers containing O-bound ligands. Such binding only weakly

perturbs the N=N bond, vibrational excitation of which occurs in this spectral region. By contrast, the spectral feature between 2300 and 2375  $\text{cm}^{-1}$  is a signature of the presence of N-bound ligands. Binding *via* the terminal N-atom has a much larger effect on both the force constant of the N=N bond and the effective reduced mass leading to the pronounced blue-shift observed in the spectrum relative to the free  $\text{N}_2\text{O}$  band at 2223.5  $\text{cm}^{-1}$ .

As is clear from Figure 4, the exact position of each spectral feature is calculated to be weakly dependent on the isomeric form. In the case of  $\text{Cu}^+(\text{N}_2\text{O})_2$  and  $\text{Au}^+(\text{N}_2\text{O})_2$ , the low wavenumber (O-bound) band in the  $\text{O}^2$  isomer is 6  $\text{cm}^{-1}$  red-shifted relative to the same feature in the  $\text{N}^1\text{O}^1$  isomer. Similarly, the N-bound band in the  $\text{N}^2$  isomers is itself 6  $\text{cm}^{-1}$  red-shifted relative to the same feature in the  $\text{N}^1\text{O}^1$  isomer. The same qualitative effect is seen in the  $\text{Ag}^+$  complex but the relative shift is smaller. The differing spectral positions in different isomers is reflected here in the width of the spectral features observed but may be resolvable as distinct peaks at higher resolution.

The linear global minimum structures yield only one active IR band in the region of interest (*i.e.*, the antisymmetric combination of N=N ligand stretches) and hence, the 2240  $\text{cm}^{-1}$  band is, in most cases, clear evidence of the presence of O-bound ligands. At this resolution, it is not possible to distinguish spectrally: i) a mixture of isomers, and ii) a pure population of the  $\text{N}^1\text{O}^1$  isomers (IIA, IIB, IIC). The former, however, is much more likely.

### **Larger complexes and spectral trends**

The range of possible  $\text{N}^x\text{O}^y$  structural combinations present scales linearly with the number of ligands. The fractional population of each isomer, and hence, the contribution to the observed IR spectrum is, however, a complicated function of the cluster growth mechanism which is highly unlikely to produce a binomial coefficient (or Pascal's triangle) distribution. For



example, by virtue of the deeper well on the potential energy landscape, a new N-bound ligand can always displace an existing O-bound ligand but the reverse is not true. Hence, the final population distribution, although not necessarily thermal, is expected to be richer in the energetically lower-lying N-bound isomers. Furthermore, it is likely that addition of a new ligand, with the increase in internal energy this brings, will lead to some annealing of the parent cluster further enriching in the lower energy structures.

In the absence of quantitative information on the isomeric distribution within our cluster beam, we have attempted to fit the IR spectra for  $n \geq 3$  complexes to a convolution of simulated spectra of contributing isomers assuming a binomial distribution of isomers. This produces satisfactory, though imperfect, agreement with the experimental IR-REPD spectra. Figure 5 shows an example of such a spectral convolution for the  $\text{Ag}^+(\text{N}_2\text{O})_3$  complex (similar simulations for a range of other complexes are given in the supporting information). Again, the isomer-specific spectral shifts of individual bands accounts for the spectral width of features observed in the spectrum (up to  $25 \text{ cm}^{-1}$  FWHM despite a IR laser resolution of  $4 \text{ cm}^{-1}$ ). We can conclusively rule out the presence of a pure distribution of either global minimum  $\text{N}^3$  isomers or indeed  $\text{O}^3$  isomers since in the  $n = 2$  case, these would both lead to a single feature in the spectrum. It is clear in this case, too, that structures containing both N- and O-bound ligands are present but we resist the temptation to infer relative abundances of each from the relative intensities of spectral bands.

The trends in the spectral shifts observed in Figure 1 as a function of complex size can be understood in terms of consideration of the valence orbitals involved in the interaction. As discussed above, the blue-shifts observed in the N-bound ligands are largest for the gold complexes followed by the copper and are smallest of all for the silver complexes. Figure 6 shows the calculated valence orbital energies of the Group 11 cations along with the LUMO ( $3\pi$ ), HOMO ( $2\pi$ ) and HOMO-1 ( $7\sigma$ ) orbitals of nitrous oxide. In  $\text{N}_2\text{O}$ , the  $7\sigma$  orbital is

antibonding with respect to the N=N bond and hence  $\sigma$ -donation from this orbital onto the metal center strengthens the N=N bond resulting in a spectral blue-shift.

Inspection of the molecular orbitals involved (see supporting information Figures S57 and S58), shows that the actual interaction of N-bound ligands is dominated by  $\sigma$ -donation to metal-centered  $s-d_z^2$  hybrid orbitals, formed from the vacant  $ns$  and the HOMO  $d_z^2$  orbital on the  $M^+$  ion. This  $s-d$  hybridization was first postulated by Orgel to account for the special stability of linear  $d^{10}$  metal cation  $M^+-L_2$  complexes relative to their tetrahedral and octahedral counterparts – in particular for  $Au^+$  complexes.<sup>43</sup> The strength of the  $M^+-N_2O$  interaction, and hence the observed spectral blue-shift, does not correlate (as might be expected) with the  $7\sigma - M^+$  LUMO gap directly. Instead, it depends on the degree of hybridization induced on the  $M^+$  ion upon complexation. In turn, this degree of hybridization depends inversely on the  $M^+$  HOMO–LUMO gap. As shown in Figure 6, the magnitude of this gap indeed follows the trend  $Au^+ \leq Cu^+ < Ag^+$  (see supporting information for more information, and Figure 7 below for ligand binding energies). The anomalously small HOMO–LUMO gap in  $Au^+$  arises from relativistic effects and is reflected in the relative stability of linear  $Au^+-L_2$  complexes compared with  $Cu^+$  and  $Ag^+$  analogues.<sup>43</sup>

Similar arguments go some way to explaining the apparent coordination numbers for each metal cation. With each successive ligand addition, the degree of  $\sigma$ -donation drops, reducing the spectral blue-shift associated with N-bound ligands. As shown in Figure 2, the reduction in blue-shift of the N-bound peak ceases at  $n = 2$  for  $Au^+$  but continues to  $n = 4$  for  $Cu^+$  and  $Ag^+$ , suggesting that these complex sizes represent something of a change in coordination.

These coordination shells are also observed in the calculated ligand dissociation energies. Figure 7 shows the calculated binding energies of successive N-bound ligands for  $Cu^+(N_2O)_n$ ,  $Ag^+(N_2O)_n$  and  $Au^+(N_2O)_n$  complexes, respectively. Evidence for strongly-bound  $M^+L_2$

structures is clear in the marked drop in binding energy for the third ligand relative to that of the first two ligands. In the case of  $\text{Cu}^+$  and  $\text{Ag}^+$ , there is a second, albeit less pronounced, drop between  $n = 4$  and 5 consistent with the trend in spectral blue-shifts and supporting the idea of a second coordination shell.

In the absence of other  $\text{M}^+(\text{N}_2\text{O})_n$  systems with which to compare, these results can most appropriately be seen in the context of recent IR studies of  $\text{M}^+(\text{NO})_n$  ( $\text{M} = \text{Cu}, \text{Ag}, \text{Au}$ ) complexes by Zhou and coworkers.<sup>44-45</sup> For the nitrosyl complexes, consistent with the present work, clear step decreases in the bond dissociation energies were observed for all coinage metal cations between  $n = 2$  and 3, with further evidence of coordination shells at  $n = 4$  for  $\text{Cu}^+$ , and  $n = 5$  for  $\text{Ag}^+$ . Furthermore, the same pattern of stronger ligand binding to  $\text{Au}^+$  and  $\text{Cu}^+$  ions than for  $\text{Ag}^+$  was observed. In fact, the core M–L binding energies in the two types of complex are surprising similar for the two ligands – more incipient chemical bonding might have been expected in the case of the open shell NO. One noteworthy difference between complexes of the two ligands is that within the nitrosyl complexes there is evidence of considerably more ligand–ligand interaction than we observe in the case of  $\text{N}_2\text{O}$  complexes.

By contrast with the above, O–bound  $\text{N}_2\text{O}$  interactions are assumed to be dominated by electrostatic interactions. Orbital overlap between the occupied  $\pi$  orbitals on the O atom of the  $\text{N}_2\text{O}$  and the unoccupied  $s$  orbitals on the metal cation is poor and the metal cation center interacts directly with one of the O atom lone pairs. This accounts for the two equivalent, non–linear O–bound minima on the potential energy surfaces. The calculated barrier (at  $180^\circ$ , see Figure 3) between the identical secondary minima is small (ranging from  $< 0.1$  eV in  $\text{Cu}^+\text{N}_2\text{O}$ , to *ca.* 0.3 eV in  $\text{Au}^+\text{N}_2\text{O}$ ), suggesting the complexes may undergo particularly large amplitude motion in this well. However, since the detected N=N stretch is largely unaffected

by this interaction, there is no clear spectral signature of this effect at the resolution employed here.

Previous studies of N<sub>2</sub>O molecularly-bound on size-selected Rh<sub>*m*</sub><sup>+</sup> and Rh<sub>*m*</sub>O<sup>+</sup> clusters have demonstrated the ability to drive reactivity by infrared-pumping of the N<sub>2</sub>O chromophore.<sup>27-29</sup> In the case of Rh<sub>*m*</sub>N<sub>2</sub>O<sup>+</sup> clusters (*m* = 4–8), the results were interpreted in terms of exclusively N-bound isomers on account of the observed blue-shift in the N–O stretching frequency (or N<sub>2</sub>O symmetric stretch) relative to that in free N<sub>2</sub>O. However, one might expect N<sub>2</sub>O decomposition to be more effective in the case of an O-binding motif given that the ultimate products are Rh<sub>*m*</sub>O<sup>+</sup> + N<sub>2</sub>. Indeed, considerable rearrangement, requiring free adjacent binding sites, was required to account for decomposition of the N-bound nitrous oxide, a pathway which has to compete with simple N<sub>2</sub>O loss.<sup>28</sup> The ability to distinguish spectrally between N-bound and O-bound ligands, as demonstrated here, offers the tantalizing prospect of driving mode-selective reactivity in different isomers.

## Conclusions

Small gas-phase nitrous oxide complexes of coinage metal cations have been studied using infrared spectroscopy in region of the ligand N=N stretch. Comparison of the experimental spectra with spectral simulations from density functional theory yields clear evidence for isomers containing N-bound and O-bound ligands with the spectral signature of the former blue-shifted from the free N<sub>2</sub>O frequency by up to 140 cm<sup>-1</sup>. The trends observed between different metal complexes M<sup>+</sup>, as well as those with increasing numbers of ligands, are interpreted on the basis of the molecular orbital picture of the binding in which the approaching ligand induces *s*–*d<sub>z</sub>*<sup>2</sup> hybridization of the M<sup>+</sup> ion.

It is comparatively unusual for the same ligand to be observed bound in multiple arrangements and the ability to selectively excite one binding motif over another may provide an opportunity to drive different intra-cluster chemistry in different isomers.

### **Supporting Information Available**

low-energy calculated structures and energies, additional potential energy surfaces, calculated binding energies.

### **Acknowledgments**

E.M.C. and A.I. are grateful to the EPSRC for graduate studentships. A.I. is similarly grateful to Wadham College, Oxford. P.M.B. thanks St. John's College, Oxford for funding of his summer research fellowship. This work is supported by EPSRC under Programme Grant No. EP/L005913. We are grateful to Advanced Research Computing (ARC) facility at the University of Oxford for providing supercomputer facilities. We are grateful to Professor John McGrady for helpful discussions regarding the molecular orbital aspects of this work.

### **Corresponding Author**

\*stuart.mackenzie@chem.ox.ac.uk

## References

1. Duncan, M. A., Infrared Spectroscopy to Probe Structure and Dynamics in Metal Ion-Molecule Complexes. *Int. Rev. Phys. Chem.* **2003**, 22 (2), 407-435.
2. Tolman, W. B., Binding and Activation of N<sub>2</sub>O at Transition-Metal Centers: Recent Mechanistic Insights. *Angew. Chemie Int. Ed.* **2010**, 49 (6), 1018-1024.
3. Castleman, A. W.; Keesee, R. G., Clusters: Bridging the Gas and Condensed Phases. *Acc. Chem. Res.* **1986**, 19 (12), 413-419.
4. Castleman, A. W.; Bowen, K. H., Clusters: Structure, Energetics, and Dynamics of Intermediate States of Matter. *J. Phys. Chem.* **1996**, 100 (31), 12911-12944.
5. Böhme, D. K.; Schwarz, H., Gas-Phase Catalysis by Atomic and Cluster Metal Ions: The Ultimate Single-Site Catalysts. *Angew. Chemie Int. Ed.* **2005**, 44 (16), 2336-2354.
6. 2009 U.S. Greenhouse Gas Inventory Report, Environmental Protection Agency (<http://tinyurl.com/emissionsreport>).
7. Prather, M. J., Time Scales in Atmospheric Chemistry: Coupled Perturbations to N<sub>2</sub>O, NO<sub>y</sub>, and O<sub>3</sub>. *Science* **1998**, 279 (5355), 1339-1341.
8. Ravishankara, A. R.; Daniel, J. S.; Portmann, R. W., Nitrous Oxide (N<sub>2</sub>O): The Dominant Ozone-Depleting Substance Emitted in the 21st Century. *Science* **2009**, 326 (5949), 123-125.
9. Kapteijn, F.; Rodriguez-Mirasol, J.; Moulijn, J. A., Heterogeneous Catalytic Decomposition of Nitrous Oxide. *App. Catal. B* **1996**, 9 (1), 25-64.
10. Lavrov, V. V.; Blagojevic, V.; Koyanagi, G. K.; Orlova, G.; Bohme, D. K., Gas-Phase Oxidation and Nitration of First-, Second-, and Third-Row Atomic Cations in Reactions with Nitrous Oxide: Periodicities in Reactivity. *J. Phys. Chem. A* **2004**, 108 (26), 5610-5624.
11. Delabie, A.; Vinckier, C.; Flock, M.; Pierloot, K., Evaluating the Activation Barriers for Transition Metal N<sub>2</sub>O Reactions. *J. Phys. Chem. A* **2001**, 105 (22), 5479-5485.
12. Stirling, A., Oxygen-Transfer Reactions between 3d Transition Metals and N<sub>2</sub>O and NO<sub>2</sub>. *J. Am. Chem. Soc.* **2002**, 124 (15), 4058-4067.
13. Kryachko, E. S.; Tishchenko, O.; Nguyen, M. T., Mechanism of the Oxidation Reaction of Cu with N<sub>2</sub>O via Nonadiabatic Electron Transfer. *Int. J. Quantum Chem.* **2002**, 89 (4), 329-340.
14. Jin, X.; Wang, G.; Zhou, M., Matrix Isolation Infrared Spectroscopic and Theoretical Study of Nickel, Palladium, and Platinum Nitrous Oxide Complexes. *J. Phys. Chem. A* **2006**, 110 (26), 8017-8022.
15. Wang, G.; Jin, X.; Chen, M.; Zhou, M., Matrix Isolation Infrared Spectroscopic and Theoretical Study of the Copper (I) and Silver (I)-Nitrous Oxide Complexes. *Chem. Phys. Lett.* **2006**, 420 (1-3), 130-134.

16. Hintz, P. A.; Ervin, K. M., Chemisorption and Oxidation Reactions of Nickel Group Cluster Anions with N<sub>2</sub>, O<sub>2</sub>, CO<sub>2</sub>, and N<sub>2</sub>O. *J. Chem. Phys.* **1995**, *103* (18), 7897-7906.
17. Dietrich, G.; Lutzenkirchen, K.; Becker, S.; Hasse, H. U.; Kluge, H. J.; Lindinger, M.; Schweikhard, L.; Ziegler, J.; Kuznetsov, S., Au<sub>n</sub><sup>+</sup> Induced Decomposition of N<sub>2</sub>O. *Ber. Bunsen-Ges. Phys. Chem. Chem. Phys.* **1994**, *98* (12), 1608-1612.
18. Balaj, O. P.; Balteanu, I.; Rossteuscher, T. T. J.; Beyer, M. K.; Bondybey, V. E., Catalytic Oxidation of CO with N<sub>2</sub>O on Gas-Phase Platinum Clusters. *Angew. Chemie Int. Ed.* **2004**, *43* (47), 6519-6522.
19. Balteanu, I.; Balaj, O. P.; Beyer, M. K.; Bondybey, V. E., Reactions of Platinum Clusters <sup>195</sup>Pt<sub>n</sub><sup>+/-</sup>, n=1-24, with N<sub>2</sub>O Studied with Isotopically Enriched Platinum. *Phys. Chem. Chem. Phys.* **2004**, *6* (11), 2910-2913.
20. Harding, D.; Ford, M. S.; Walsh, T. R.; Mackenzie, S. R., Dramatic Size Effects and Evidence of Structural Isomers in the Reactions of Rhodium Clusters, Rh<sub>n</sub><sup>+/-</sup>, with Nitrous Oxide. *Phys. Chem. Chem. Phys.* **2007**, *9* (17), 2130-2136.
21. Anderson, M. L.; Lacz, A.; Drewello, T.; Derrick, P. J.; Woodruff, D. P.; Mackenzie, S. R., The Chemistry of Nitrogen Oxides on Small Size-Selected Cobalt Clusters, Co<sub>n</sub><sup>+</sup>. *J. Chem. Phys.* **2009**, *130* (6).
22. Parry, I. S.; Kartouzian, A.; Hamilton, S. M.; Balaj, O. P.; Beyer, M. K.; Mackenzie, S. R., Collisional Activation of N<sub>2</sub>O Decomposition and CO Oxidation Reactions on Isolated Rhodium Clusters. *J. Phys. Chem. A* **2013**, *117* (36), 8855-8863.
23. Beyer, M. K.; Berg, C. B.; Bondybey, V. E., Gas-Phase Reactions of Rhenium-Oxo Species ReO<sub>n</sub><sup>+</sup>, n=0, 2-6, 8, with O<sub>2</sub>, N<sub>2</sub>O, CO, H<sub>2</sub>O, H<sub>2</sub>, CH<sub>4</sub> and C<sub>2</sub>H<sub>4</sub>. *Phys. Chem. Chem. Phys.* **2001**, *3* (10), 1840-1847.
24. Rodgers, M. T.; Walker, B.; Armentrout, P. B., Reactions of Cu<sup>+</sup>(<sup>1</sup>S and <sup>3</sup>D) with O<sub>2</sub>, CO, CO<sub>2</sub>, N<sub>2</sub>, NO, N<sub>2</sub>O, and NO<sub>2</sub> Studied by Guided Ion Beam Mass Spectrometry. *Int. J. Mass Spectrom.* **1999**, *182*, 99-120.
25. Inokuchi, Y.; Matsushima, R.; Kobayashi, Y.; Ebata, T., Ion Core Structure in (N<sub>2</sub>O)<sub>n</sub><sup>+</sup> (n=2–8) Studied by Infrared Photodissociation Spectroscopy. *J. Chem. Phys.* **2009**, *131* (4), 044325.
26. Thompson, M. C.; Weber, J. M., Infrared Spectroscopic Studies on the Cluster Size Dependence of Charge Carrier Structure in Nitrous Oxide Cluster Anions. *J. Chem. Phys.* **2016**, *144* (10), 104302.
27. Hamilton, S. M.; Hopkins, W. S.; Harding, D. J.; Walsh, T. R.; Gruene, P.; Haertelt, M.; Fielicke, A.; Meijer, G.; Mackenzie, S. R., Infrared Induced Reactivity on the Surface of Isolated Size-Selected Clusters: Dissociation of N<sub>2</sub>O on Rhodium Clusters. *J. Am. Chem. Soc.* **2010**, *132* (5), 1448-1449.

28. Hamilton, S. M.; Hopkins, W. S.; Harding, D. J.; Walsh, T. R.; Haertelt, M.; Kerpel, C.; Gruene, P.; Meijer, G.; Fielicke, A.; Mackenzie, S. R., Infrared-Induced Reactivity of N<sub>2</sub>O on Small Gas-Phase Rhodium Clusters. *J. Phys. Chem. A* **2011**, *115* (12), 2489-2497.
29. Hermes, A. C.; Hamilton, S. M.; Hopkins, W. S.; Harding, D. J.; Kerpel, C.; Meijer, G.; Fielicke, A.; Mackenzie, S. R., Effects of Coadsorbed Oxygen on the Infrared Driven Decomposition of N<sub>2</sub>O on Isolated Rh<sub>5</sub><sup>+</sup> Clusters. *J. Phys. Chem. Lett.* **2011**, *2* (24), 3053-3057.
30. Parry, I. S.; Kartouzian, A.; Hamilton, S. M.; Balaj, O. P.; Beyer, M. K.; Mackenzie, S. R., Chemical Reactivity on Gas-Phase Metal Clusters Driven by Blackbody Infrared Radiation. *Angew. Chemie Int. Ed.* **2015**, *54* (4), 1357-1360.
31. Jellinek, J.; Guvenc, Z. B., Mode Selectivity in Cluster-Molecule Interactions - Ni<sub>13</sub> + D<sub>2</sub>. In *Mode Selective Chemistry*, Jortner, J.; Levine, R. D.; Pullman, B., Eds. Kluwer Academic Publ: Dordrecht, 1991; Vol. 24, pp 153-164.
32. Lisy, J. M., Spectroscopy and Structure of Solvated Alkali-Metal Ions. *Int. Rev. Phys. Chem.* **1997**, *16* (3), 267-289.
33. Cabarcos, O. M.; Weinheimer, C. J.; Lisy, J. M., Size Selectivity by Cation- $\pi$  Interactions: Solvation of K<sup>+</sup> and Na<sup>+</sup> by Benzene and Water. *J. Chem. Phys.* **1999**, *110* (17), 8429-8435.
34. Rodriguez, O.; Lisy, J. M., Infrared Spectroscopy of Li<sup>+</sup>(CH<sub>4</sub>)<sub>1</sub>Ar<sub>n</sub>, n = 1-6, Clusters. *J. Phys. Chem. A* **2011**, *115* (7), 1228-1233.
35. Iskra, A.; Gentleman, A. S.; Kartouzian, A.; Kent, M. J.; Sharp, A. P.; Mackenzie, S. R., Infrared Spectroscopy of Gas-Phase M<sup>+</sup>(CO<sub>2</sub>)<sub>n</sub> (M = Co, Rh, Ir) Ion-Molecule Complexes. *J. Phys. Chem. A* **2017**, *121* (1), 133-140.
36. Knickelbein, M. B.; Menezes, W. J. C., Metal Cluster-Rare Gas van der Waals Complexes: Physisorption on a Microscopic Scale. *J. Phys. Chem.* **1992**, *96* (16), 6611-6616.
37. Ayotte, P.; Weddle, G. H.; Kim, J.; Johnson, M. A., Vibrational Spectroscopy of the Ionic Hydrogen Bond: Fermi Resonances and Ion-Molecule Stretching Frequencies in the Binary X-H<sub>2</sub>O (X = Cl, Br, I) Complexes via Argon Predissociation Spectroscopy. *J. Am. Chem. Soc.* **1998**, *120* (47), 12361-12362.
38. Perdew, J. P., Density-Functional Approximation for the Correlation Energy of the Inhomogeneous Electron Gas. *Phys. Rev. B* **1986**, *33* (12), 8822-8824.
39. Weigend, F.; Ahlrichs, R., Balanced Basis Sets of Split Valence, Triple Zeta Valence and Quadruple Zeta Valence Quality for H to Rn: Design and Assessment of Accuracy. *Phys. Chem. Chem. Phys.* **2005**, *7* (18), 3297-3305.
40. Weigend, F., Accurate Coulomb-Fitting Basis Sets for H to Rn. *Phys. Chem. Chem. Phys.* **2006**, *8* (9), 1057-1065.



41. Frisch, M. J.; Trucks, G. W.; Schlegel, H. B.; Scuseria, G. E.; Robb, M. A.; Cheeseman, J. R.; Scalmani, G.; Barone, V.; Mennucci, B.; Petersson, G. A.; et al., Gaussian 09, Revision B.01. *Gaussian 09, Revision B.01, Gaussian, Inc., Wallingford CT* **2009**.
42. Herzberg, G., *Molecular Spectra and Molecular Structure: II Infrared and Raman Spectra of Polyatomic Molecules*. Krieger: Malabar, Florida, 1991; Vol. 2.
43. Orgel, L. E., 843. Stereochemistry of Metals of the B Sub-Groups. Part I. Ions with Filled d-Electron Shells. *J. Chem. Soc.* **1958**, 4186-4190.
44. Li, Y.; Wang, L.; Qu, H.; Wang, G.; Zhou, M., Infrared Photodissociation Spectroscopy of Mass-Selected Silver and Gold Nitrosyl Cation Complexes. *J. Phys. Chem. A* **2015**, *119* (15), 3577-3586.
45. Wang, L.; Wang, G.; Qu, H.; Li, Z. H.; Zhou, M., Flexible Bonding Between Copper and Nitric Oxide: Infrared Photodissociation Spectroscopy of Copper Nitrosyl Cation Complexes:  $[\text{Cu}(\text{NO})_n]^+$  ( $n = 1-5$ ). *Phys. Chem. Chem. Phys.* **2014**, *16* (22), 10788-10798.

## Figures

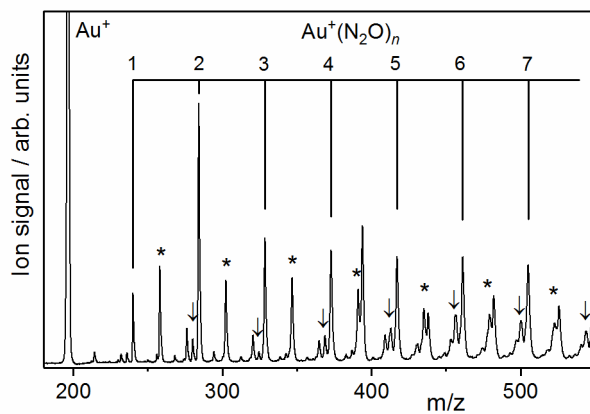


**Figure 1.** Time of flight mass spectrum of  $\text{Au}^+(\text{N}_2\text{O})_n$  complexes produced by ablation of a gold target in an argon carrier gas seeded with 0.6 %  $\text{N}_2\text{O}$ . Ar-tagged peaks are indicated by arrows. Asterisks (\*) mark mixed  $\text{N}_2\text{O} / \text{H}_2\text{O}$  complexes not considered here and pure  $(\text{N}_2\text{O})_n^+$  complexes are also present.

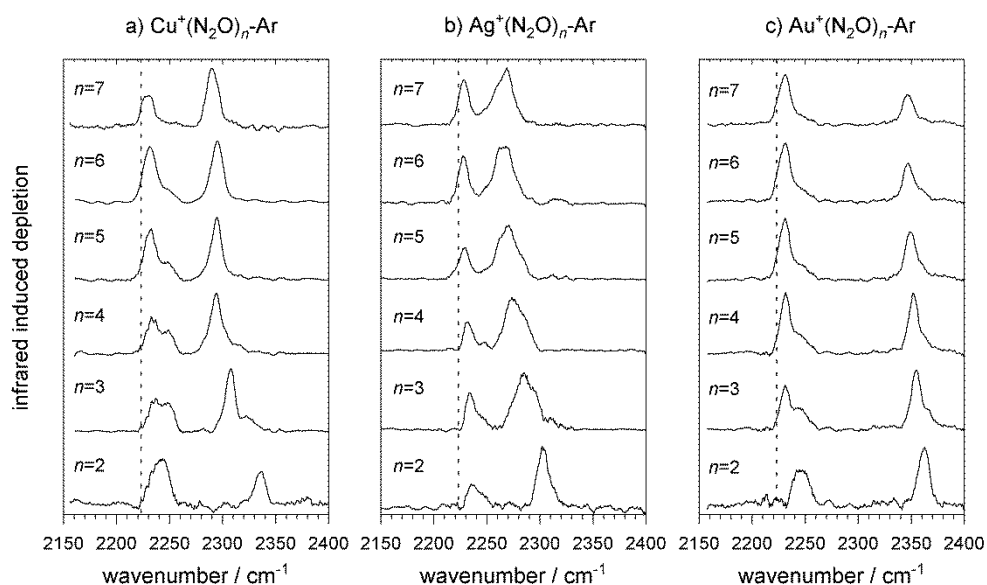


**Figure 2.** Infrared depletion spectra of  $M^+(N_2O)_n-Ar$  ( $n=2-7$ ) complexes ( $M =$  a) Cu, b) Ag and c) Au) showing two distinct spectral features. In each case depletion occurs due to the loss of the Ar messenger atom. For ease of comparison the depletion intensity for each spectrum has been normalized with the maximum value in this region. The dashed line indicates the wavenumber of the  $\nu_3$  (N=N stretching) mode in isolated  $N_2O$  at  $2223.5\text{ cm}^{-1}$ .<sup>42</sup>

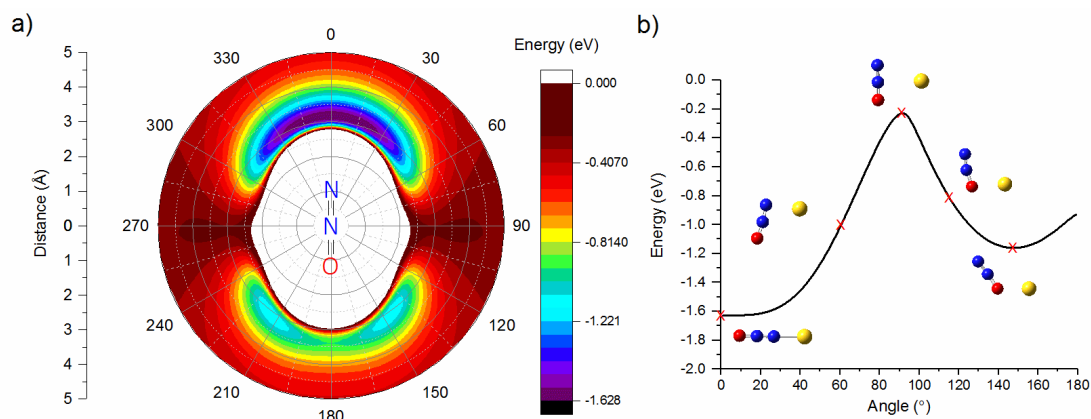


**Figure 3** a) Potential energy surface for the  $\text{Au}^+\text{N}_2\text{O}$  complex showing a linear  $\text{Au}^+\text{NNO}$  global minimum structure and a secondary, bent,  $\text{Au}^+\text{ONN}$  minimum structure. This surface was generated by fixing the  $\text{N}_2\text{O}$  molecule at its equilibrium geometry. b) Minimum energy pathway as a function of bond angle illustrating the relative energies of N-bound and O-bound minima. For this purpose the  $\text{N}_2\text{O}$  geometry was relaxed. The equivalent potential energy surfaces of the  $\text{Cu}^+\text{N}_2\text{O}$  and  $\text{Ag}^+\text{N}_2\text{O}$  complexes are qualitatively similar (see supporting information).

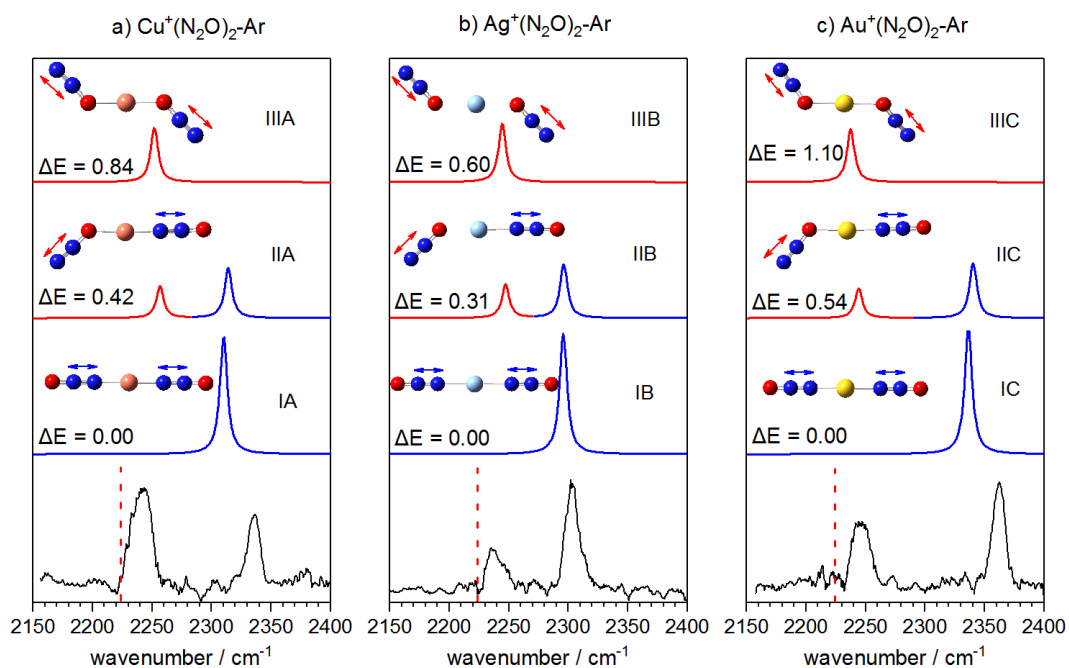


**Figure 4.** Comparison of experimental infrared depletion spectra of  $M^+(N_2O)_2-Ar$  complexes ( $M = a) Cu, b) Ag$  and  $c) Au$ ), with simulated vibrational spectra of energetically low-lying isomers. Bands in blue correspond to N=N stretches in N-bound  $N_2O$  ligands and those in red to O-bound ligands. Relative energies are given in eV. The dashed line indicates the wavenumber of the  $\nu_3$  (N=N stretching) mode in isolated  $N_2O$  at  $2223.5\text{ cm}^{-1}$ .<sup>42</sup>

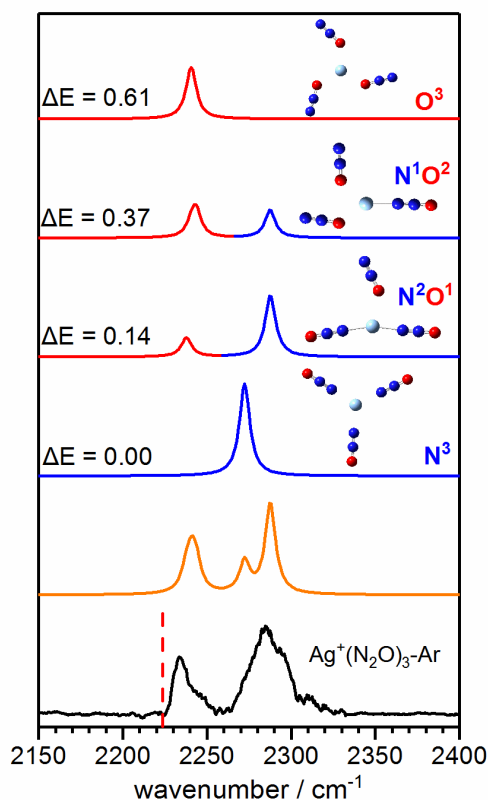


**Figure 5.** Experimental infrared depletion spectrum of  $\text{Ag}^+(\text{N}_2\text{O})_3\text{-Ar}$  complex along with simulated IR spectra of energetically low-lying isomers in the N=N stretching region. **Blue:** Simulated IR bands correspond to N-bound  $\text{N}_2\text{O}$  ligands, and **Red:** Simulated IR bands corresponding to O-bound ligands. **Orange:** combined IR spectrum assuming a 1:3:3:1 weighting of the four isomers. The relative energies of the isomers concerned are given in eV. The dashed line indicates the wavenumber of the  $\nu_3$  (N=N stretching) mode in isolated  $\text{N}_2\text{O}$  at  $2223.5\text{ cm}^{-1}$ .<sup>42</sup>

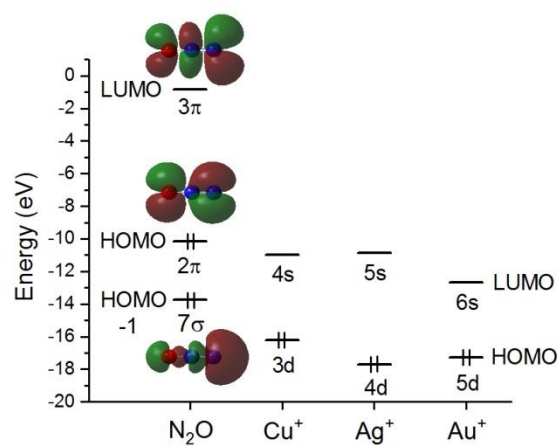


**Figure 6.** Relevant valence orbital energies calculated from density functional theory (B3P86/Def2TZVP) of Cu<sup>+</sup>, Ag<sup>+</sup>, Au<sup>+</sup>. Energies of the orbitals of N<sub>2</sub>O are shown for comparison. Energies are in eV.

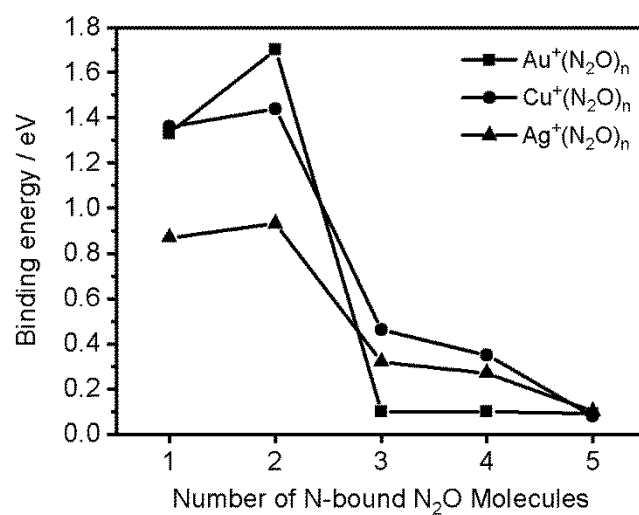


**Figure 7:** Successive ligand binding energies of N-bound  $M^+(N_2O)_n$  complexes calculated as  $E[M^+(N_2O)_n] - E[M^+(N_2O)_{n-1}] - E[N_2O]$  including zero point correction.



